Influence of the macro-porosity and the meso-structure on the dynamic properties of concrete

Fabrice Gatuingt, Silvère Pierre

Influence of the macro-porosity and the meso-structure on the dynamic properties of concrete

F. Gatuingt & S. Pierre
LMT-Cachan, ENS Cachan / CNRS / UniverSud Paris, 61 avenue du Président Wilson, F-94235 Cachan, France

ABSTRACT : Traditionally, the variability of concrete properties (in statics) is represented - in classical macroscopic models - using stochastic tools that can be complex and have to be identify with a large number of experimental tests. However, this phenomenon is usually linked to a "deterministic" characteristic of the material : the multiple defaults that can be found in the cement paste matrix. This works intends to explore the influence of the heterogeneous meso-structure coupled with an explicit representation of the macro-porosity on the dynamic properties of concrete like material. For this purpose we use FE simulations with a cohesive approach and an explicit representation of the meso-structure, including macro-pores in the cement paste. In this kind of material, heterogeneities (in our case the biggest aggregates) have sizes of the order of tens of millimeters with defaults (pores) in the matrix we can imagine that they will influence fracture properties. To obtain a realistic description of the meso-structure we used a distribution of the aggregate according to the Fuller distribution (Fuller & Thompson 1907) and the distribution of the macro-porosity is computed by analyzing images of real concrete specimens obtained by X-ray microtomography.

1 INTRODUCTION

The aim of this study is to analyze the dynamic behavior of concrete with FE simulations using a cohesive approach and an explicit representation of the meso-structure including macro-pores in the cement paste. The distribution of the macro-porosity is computed by analyzing images of real concrete specimens obtained by X-ray microtomography. With this description we intend to explore the influence of the heterogeneous meso-structure coupled with an explicit representation of the macro-porosity on the dynamic properties of concrete like material. For this purposes 2D geometrical models of concrete consisting of aggregates, interfacial transition zones and a matrix (with holes) are generated. For the simulations, we use a finite element framework with cohesive elements to explicitly represent the crack nucleation and growth. The debonding process in the cohesive elements is controlled by a traction separation law based on the popular linear extrinsic irreversible law proposed by (Camacho & Ortiz 1996).
We validate our model by simulating direct dynamic tension tests of concrete specimens. The role of the meso-structure and the influence of the loading rate are then analyzed. We especially focus on the evolution of the stress peak and the dissipated energy. We can observe that with a traction separation law independent of the strain rate we are not able to reproduce the macroscopic rate effect experimentally observed while the global dissipated energy is correctly predicted. We will also show the respective influences of the meso-structure and the loading rate on the variability of the peak stress in tension. We finally attempt to give some results on the scale effects in dynamics with various sizes of our specimens.

2 MESO-STRUCTURE GENERATION

2.1 *Meso-structure description*

The meso-scale allows representing the biggest heterogeneities and provides a way to better understand the internal failure mechanisms in the materials. For these reasons, the choice of the phases represented in the meso-structure is assumed to be important to preserve the physical meaning of simulations such as the ones presented hereafter. The choice made here is to represent only the millimetric porosity and the aggre-

gates larger than these pores. The inclusions, both aggregates and pores, are discretized in classes of identical radius, based on a distribution function (the Fuller curve for the aggregates), as in (Cusatis 2011) :

$$F(d_i) = \left(\frac{d_i}{d_m ax}\right)^n \tag{1}$$

Where d_i (i=1,...,N) are the diameters of the inclusions classes, $d_{max} = d_N$ is the largest inclusions class diameter and $n = 0,5$

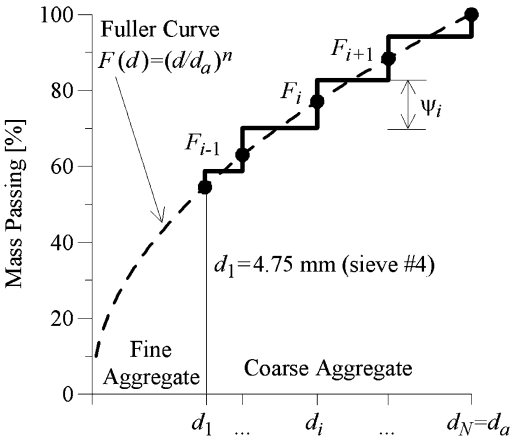

FIGURE 1: Discretization of the aggregates sizes distribution

As shown in Figure 1, inclusions smaller than d_1 will not be represented (Cusatis et al. 2006).

This discretization is computed as follow :

$$\begin{cases} \Psi_i = \dfrac{F_{i+1} - F_{i-1}}{2} & (i = 2, \ldots, N-1) \\ \Psi_1 = \dfrac{F_2 - F_1}{2} \\ \Psi_N = \dfrac{F_N - F_{N-1}}{2} \end{cases} \tag{2}$$

Where : Ψ_i is the ratio of the d_i diameter class inclusions volume over the total inclusions volume and $F_i = F(d_i)$ is the fraction of the d_i diameter class.

It is clear that knowing the total granular fraction and the Ψ_i for each of the represented class is sufficient to define the classes.

2.2 *Pores distribution*

The two types of inclusions are discretized separately for the sake of simplicity. This choice implied the strong hypothesis that a cumulative distribution function similar to the Fuller curve for the aggregates could be obtained for the macro-porosity. It is classical to use a Mercury Intrusion Porosimetry test to obtain the pores size, volume, density and other porosity-related characteristics of a material. But in our case, the assumption of a millimetric porosity implies that it is not possible to obtain these pore distribution through this test as the pores are too wide (and not connected anyway). From our knowledge, the data we are interested in are not available for classical concrete. What can be found is related to pervious concrete in cold weather climates and to the frost resistance of concrete. In these concretes macropores result from entrained air. This parameter can be controlled in the process of concrete production provided that concrete will be subjected to freeze-thaw cycles (Cordon 1966). Unfortunately in these studies, only the total porosity of concrete was determined by concrete density volume for instance. This fact led us approximate a macro-pore distribution curve computed through the post-treatment of X-ray tomography images of real concrete specimens (see Figure 2) .

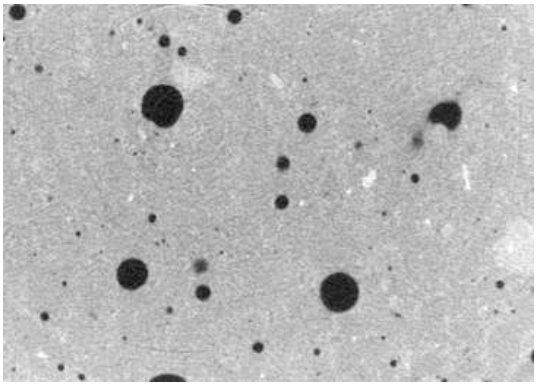

FIGURE 2: Original tomography image

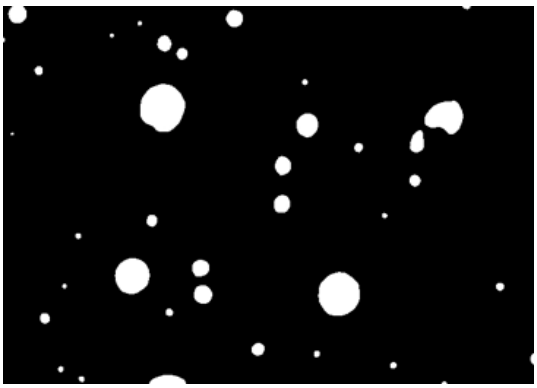

FIGURE 3: Modified tomography image obtained from Figure 2

The raw images from the tomography (Figure 2) are filtered using some native Matlab tools to bina-

rize it (Figure 3). To the resulting images is then applied a fire-propagation-like algorithm to identify the pores. The output of this identification is the number of voxels constituting each pores. We finally use the strong assumption that all the macro-pores are spherical that allows us to compute an equivalent radius for each pore. From this last operation, the expected cumulative density function can be obtained (see Figure 4) :

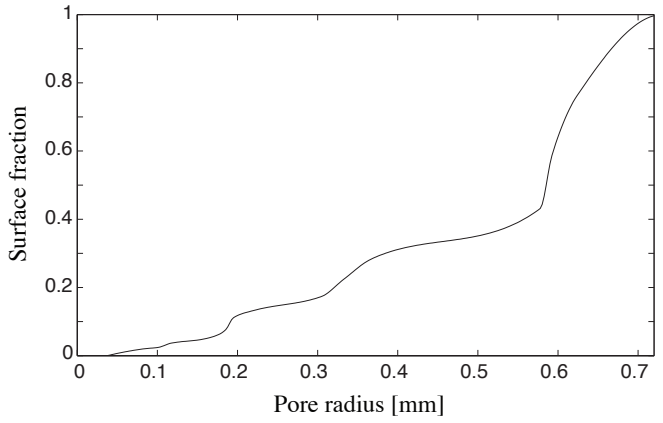

FIGURE 4: Porous cumulative density function

Based on these results only two classes of pores are necessary to represent the 3,42% porosity (see Table 1).

TABLE 1: Pores distribution obtained

Radius [mm]	0.7	0.5
Surface fraction [%]	0.85	0.85

For the aggregates, the represented classes are in Table 2.

TABLE 2: Aggregates distribution

Radius [mm]	7	6.25	5	4
Surface fraction [%]	2.38	3.98	16.71	14.32

2.3 *Meso-structure generation*

In order to distribute the inclusions over the surface of the specimen, the algorithm introduced by (Bažant et al. 1990) was used. Using this algorithm, the placing of the inclusions obeys a simple uniform random draw for the spatial coordinates until the fraction of each inclusions class is achieved. The position is checked for interferences with inclusions already in place and another position is drawn if necessary until a valid one is found. In order to fit the larger inclusions easily and optimize the accuracy, the classes are completed from the largest to the smallest diameter.
Despite its simplicity, this algorithm guarantees the isotropic distribution of each inclusions class and in our case it is accurate enough. Figure 5 shows the relative error (volume fraction generated/volume fraction expected) for different sizes of the specimen generated normalized with the diameter of the biggest aggregate. We can see on this Figure that when the specimen is larger than five time this diameter, the error of the algorithm is lower than 5%. The discrepancy plotted corresponds to different mesh generation with the same parameters.
In order to study the influence of the macro-porosity on the dynamic properties of concrete, the same meso-structure is generated with and without pores in order to have the same aggregates arrangement in both cases.

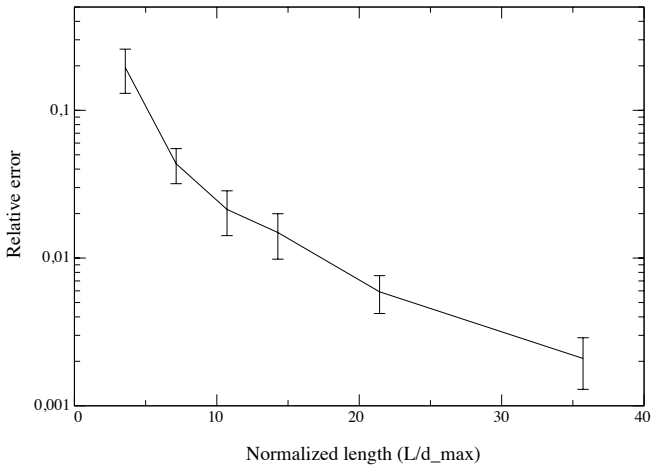

FIGURE 5: Relative error on the granular fraction generated

We can notice that we have to use this algorithm with precaution for later studies using denser inclusions structures. Likewise, for large structures this choice of algorithm might be very expensive in term of calculation time.

3 NUMERICAL SIMULATION

3.1 *F.E. mesh generation*

For the numerical simulations presented in the next section, we have to generate conforming FE mesh with 6-nodes triangular elements in 2D. The finite element code used for this study is based on a Newmark explicit time integration scheme. This scheme is conditionally stable so that the time step has to be smaller than a critical value fonction of the element

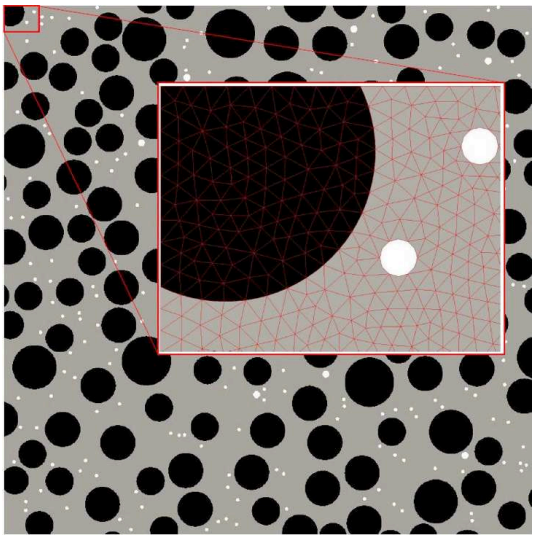

FIGURE 6: Example of a mesh of a meso-structure with pores

size (Courant–Friedrichs–Lewy condition). That is why it is important to be able to control the size of the smallest element in the FE mesh. In order to generate this mesh, we use the GMSH software (Geuzaine & Remacle 2009). The algorithm creating the geometry of the meso-structure outputs GMSH-readable files containing all the settings for the meshing. The algorithm used is the common Delaunay two dimensional meshing algorithm and the size of the elements is chosen to be between 3 to 4 times smaller than the smallest inclusion diameter. A finer meshing would not increase significantly the accuracy of the results as shown by (Gatuingt et al. 2013). It should be noted that the mesh fits the interfaces so that the elements each belong to only one material. This is also a requirement for the cohesive model used here. Figure 6 shows a zoom on a part of a mesh where an aggregate and two pores are shown.

3.2 *Cohesive approach*

As it has been mentioned before, the numerical framework used in this study is a Finite Element Method using an extrinsic cohesive approach. The cohesive element method allows us to model dynamic crack propagation and damage in a brittle material like concrete. The fracture process is described by the cohesive approach (introduced by Dugdale (Dugdale 1960) and Barenblat (Barenblatt 1962) in the 1960s) as a separation process occurring at the crack tip in a small region of material called cohesive zone. This can be introduced into a standard finite element environment using interface elements with null thickness and with a fracture-based constitutive law. We assume that the bulk material outside the cohesive zone remains elastic. In our case the crack path is not known *a priori* and all lines in the mesh are considered as a potential crack path. During the simulation, the stress at the interface between two adjacent continuum elements is computed and compared to the fracture criterion at the end of every time step. The interfacial stress, σ, is calculated averaging stresses of the adjacent Gauss points of the two continuum elements. If the inter-element stress exceeds the critical stress value, the nodes located at the inter-element boundary are doubled, the two elements are topologically disconnected and a cohesive element is inserted (see Figure 7). After the nodal disconnection, the interfacial stress starts being controlled by the traction separation law implemented in the cohesive element (Figure 8).

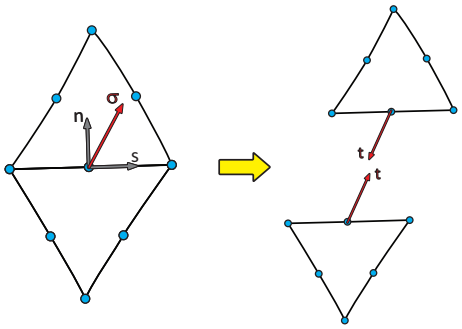

FIGURE 7: Schematic of the nodal disconnection between two continuum elements in which the interfacial stress has exceeded the critical stress

The coupling of the above mentioned fracture criterion together with an initially rigid cohesive law allows capturing the initiation of new cracks without an *a priori* definition of the possible cracks. Nevertheless, the cracks are constrained to propagate following the inter-element boundaries and the fineness of the mesh can affect it. The law we use is the linear irreversible softening law proposed by (Camacho & Ortiz 1996). The traction separation law only depends on the effective scalar displacement δ :

$$\delta = \sqrt{\Delta_n^2 + \beta^2 \Delta_s^2} \tag{3}$$

where $\overrightarrow{\Delta} = (\Delta_n, \Delta_s)$ is the relative displacement vector and the parameter β accounts for the coupling between normal and tangential displacements. The value of β has to be estimated (e.g. by correlating experimental results with numerical simulations (Ruiz, Pandolfi, & Ortiz 2001)) but it has been shown by (Snozzi, Caballero, & Molinari 2011) that the peak strength is only slightly affected by β for a tensile loading. Its value has been kept to one in this study. The cohesive tractions law is then :

$$\overrightarrow{t} = \frac{t}{\delta}(\Delta_n \overrightarrow{n} + \beta^2 \Delta_s \overrightarrow{s}) \quad (4)$$

where t represents an effective cohesive traction. This traction in case of crack opening is given by :

$$t = f_{ct}\left(1 - \frac{\delta}{\delta_c}\right) \quad \text{for} \quad \delta = \delta_{max} \quad \text{and} \quad \dot{\delta} > 0 \quad (5)$$

Where f_{ct} represents the local material strength and δ_c represents the effective relative displacement beyond which complete decohesion occurs. Whereas for crack closure or reopening (δ smaller than δ_{max}) the functional form is assumed to have the form :

$$t = \frac{\delta}{\delta_{max}} t_{max} \quad \text{for} \quad \delta < \delta_{max} \quad (6)$$

where t_{max} is the value of the effective traction when δ is equal to δ_{max}, in which is stored the maximal effective opening displacement attained up to the moment. Moreover δ_{max} also accounts for the irreversibility of the law allowing successive loading, unloading and reloading. The evolution of the linear decreasing law is graphically shown in Figure 8. Note that the definition of f_{ct} and δ_c implicitly establishes the existence of an effective fracture energy G_c, which corresponds to the area under the curve of Figure 8 :

$$G_c = \frac{1}{2} f_{ct} \delta_c \quad (7)$$

Partially damaged cohesive elements have dissipated an energy $W < G_c$. As the present work is focused on tensile uniaxial loading, the fracture energy of the different phases of our concrete is identified to the experimental one for Mode I, i.e. $G_c = G_c^I$.

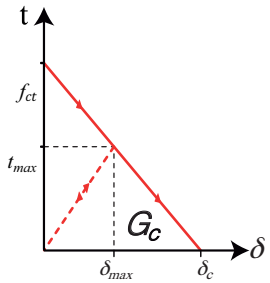

FIGURE 8: Representation of the linear cohesive law.

3.3 *Dynamic direct tension test*

To analyze the dynamic tensile response of a concrete specimen (2D plane strain), the specimen is loaded under displacement control with an imposed strain rate $\dot{\varepsilon}$. All the nodes of the finite element mesh which are located on the upper (respectively lower) boundary moved at a constant velocity V_0 :

$$V_0 = \dot{\varepsilon} \frac{h}{2} \quad (8)$$

where h is the height of the studied specimen. To avoid stress wave propagation and an early fracture near the boundaries, all the nodes of the finite element mesh are prescribed an initial velocity in accordance to their vertical position y (Miller et al. 1999) as illustrated in Figure 9 :

$$V_y(y) = \frac{2V_0}{h} y \quad (9)$$

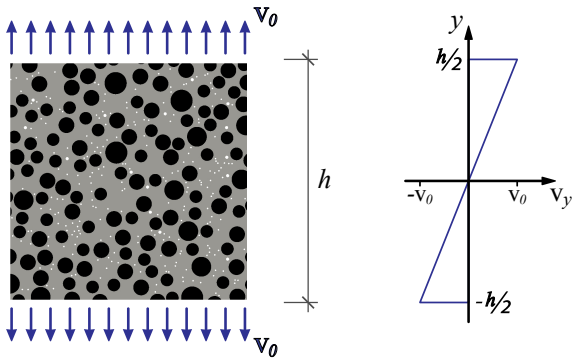

FIGURE 9: Velocity initial condition

3.4 *Results obtained*

In our simulations we decided to simulate four strain rates $\dot{\varepsilon}$ = 0.1, 1., 10. and 100. $/s$. Due to our explicite time integration scheme we are not able to compute a real quasi-static test and we assume that $\dot{\varepsilon}$ = 0.1 is close enough to this test.

Figure 10 shows the response of dynamic tension tests performed on a $15 \times 15\ cm^2$ specimen. We can see that with our approach we are able to obtain a rate effect in the result of this test without any rate effect in the constitutive laws as already shown in (Gatuingt et al. 2013). This rate effect is only due to the transition of a single crack for law strain rate to diffuse cracking for higher one as shown by comparing Figure 11 and Figure 12.

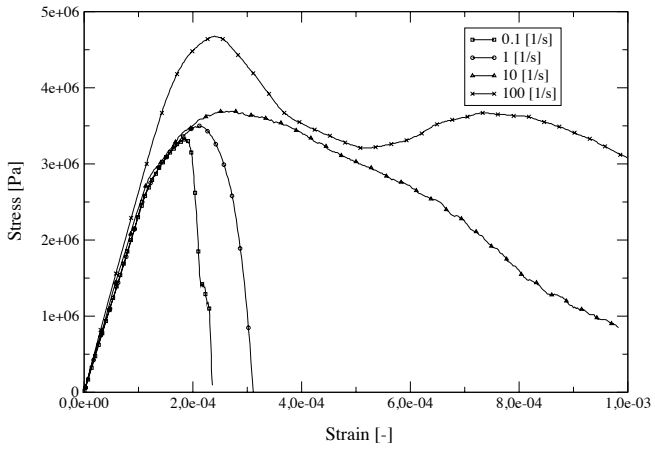

FIGURE 10: Stress-Strain responses in tension for different strain rates

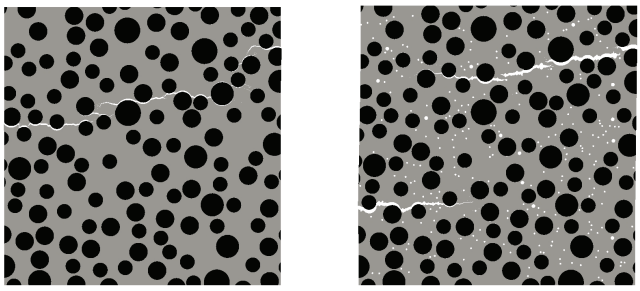

FIGURE 11: Cracks path for $\dot{\varepsilon}$ = 0.1/s for the sample without and with pores

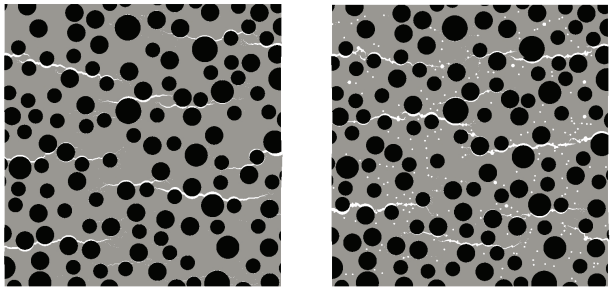

FIGURE 12: Cracks path for $\dot{\varepsilon}$ = 10/s for the sample without and with pores

We can also notice in Figure 11 and Figure 12 that the macro-pores clearly influence the cracks path both

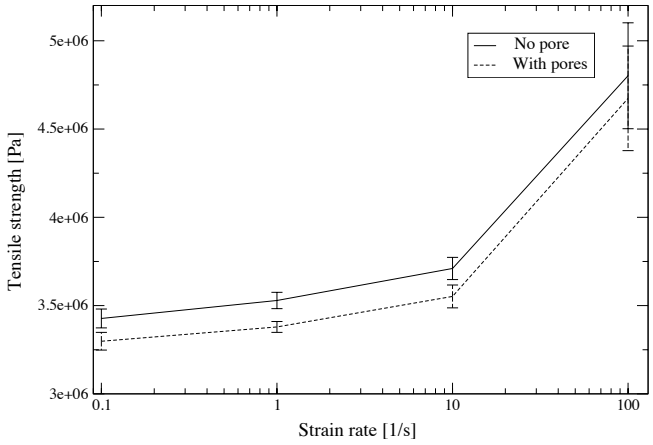

FIGURE 13: Rate effect on the tensile strength obtained without and with pores in the sample tested

for the case of a single crack ($\dot{\varepsilon}$ = 0.1/s) and for the case of diffuse cracks ($\dot{\varepsilon}$ = 10/s). This effect modifies the tensile strength obtained in the same sample depending on the presence of pores as expected. But the global influence of the porosity is not yet totally clear. Figure 13 shows the influence of the porosity on the rate effect for a $15 \times 15\ cm^2$ sample. We can see on this Figure that the tensile strength is lower with pores but the evolution of the curve seems to be the same without and with pores. But we have to conclude with precaution due to the discrepancy (several meso-structure generations) of the results at $\dot{\varepsilon}$ = 100/s in the same range of the effect of the porosity.

4 CONCLUSION

In this work we proposed a meso-scopic model for the analysis of dynamic tensile failure of concrete. This model is based on a 2D finite element description with cohesive capability of a mix of aggregates in a mortar paste matrix without and with macro-pores. The influence of the heterogeneous meso-structure and of the porosity of concrete and the loading rate on the tensile response have been studied. With our specimen size we observed a small impact of the aggregates arrangement on the tensile strength for the smallest strain rates and a more important one at $\dot{\varepsilon}$ = 100/s. The porosity clearly influenced the tensile strength but its effects on other aspects of fracture is no so clear up to now. It will be interesting to investigate in more details the influence of the porosity to see if we will be able to obtain a kind of "Weibull" response of our specimens.

Références

Barenblatt, G. (1962). The mathematical theory of equilibrium of cracks in brittle fracture. *Advances in Applied Mechanics 7*, 55–129.

Bažant, Z., M. Tabbara, M. Kazemi, & G. Pijaudier-Cabot (1990). Random particle model for fracture of aggregate or fiber composites. *Journal of Engineering Mechanics-ASCE 116*, 1686–1705.

Camacho, G. & M. Ortiz (1996). Computational modelling of impact damage in brittle materials. *International Journal of Solids and Structures 33*(20-22), 2899–2938.

Cordon, W. (1966). *Freezing and Thawing of Concrete- mechanisms and Control*. Monograph 3, American Concrete Institute.

Cusatis, G. (2011). Lattice discrete particle model (ldpm) for failure behavior of concrete. i : Theory. *Cement and Concrete Composites*, 881–890.

Cusatis, G., Z. Bažant, M. Tabbara, & L. Cedolin (2006). Confinement-shear lattice csl model for fracture propagation in concrete. *Comput. Methods Appl. Mech. Engrg 195*, 7154–7171.

Dugdale, D. (1960). Yielding of steel sheets containing slits. *Journal of the Mechanics and Physics of Solids 8*, 100–108.

Fuller, W. & S. Thompson (1907). The laws of proportioning concrete. *ASCE J. Transport.*, 67–143.

Gatuingt, F., L. Snozzi, & J. Molinari (2013). Numerical determination of the tensile response and the dissipated fracture energy of concrete : role of the mesostructure and influence of the loading rate. *Int. J. Numer. Anal. Meth. Geomech. 37*, 3112–3130.

Geuzaine, C. & J.-F. Remacle (2009). Gmsh : a three-dimensional finite element mesh generator with built-in pre- and post-processing facilities. *International Journal for Numerical Methods in Engineering 79*, 1309–1331.

Miller, O., L. Freund, & A. Needleman (1999). Modeling and simulation of dynamic fragmentation in brittle materials. *International Journal of Fracture 96*(2), 101–125.

Ruiz, G., A. Pandolfi, & M. Ortiz (2001). Three-dimensional cohesive modeling of dynamic mixed-mode fracture. *Int. Journal for Numerical Methods in Engineering 52*, 97–120.

Snozzi, L., A. Caballero, & J. Molinari (2011). Influence of the meso-structure in dynamic fracture simulation of concrete under tensile loading. *Cement and Concrete Research 41*(11), 1130–1142.